Research Article

Sibel İla, Azmi Seyhun Kipcak, and Emek Moroydor Derun*

Ultra-fast and effective ultrasonic synthesis of potassium borate: Santite

https://doi.org/10.1515/mgmc-2022-0004
received November 02, 2021; accepted February 22, 2022

Abstract: In this study, a potassium borate compound of santite is synthesized at 60°C, 70°C, 80°C, and 90°C reaction temperature for 2.5, 5, 10, and 15 min reaction time by using eight different raw material combinations of K_2CO_3, KNO_3, NaOH, H_3BO_3, B_2O_3, $Na_2B_4O_9{\cdot}5H_2O$, and $Na_2B_4O_9{\cdot}10H_2O$. According to the X-ray diffraction analysis synthesized potassium borate compound is identified as "santite ($KB_5O_8{\cdot}4H_2O$)" with powder diffraction file no. 01-072-1688. Raman spectroscopy results showed that the synthesized compound consists of typical boron mineral bands, and the spectra obtained were in mutual agreement with potassium borate, according to the literature. Scanning electron microscopic morphologies showed that obtained santite has different particle shapes as the raw material combination changed and the particle sizes are found between 305 nm and 2.03 µm. Overall reaction yields are found between 76.11% and 99.26%, even such lower reaction times with respect to the literature.

Keywords: particle size, potassium borate, reaction yield, santite, ultrasonic synthesis

1 Introduction

Metal borates, which are formed by the complex combination of boron, hydrogen, oxygen, and metal atoms, are commonly found in the anhydrous or hydrated form on earth and can be easily synthesized in the laboratory. Metal borates are used in many fields such as glass-making, chemistry, cosmetics, metallurgy, nuclear, ceramics, space, and aviation. Potassium borates are also emerging as a subclass of metal borates and are used in many fields such as glass fiber, cement, nonlinear optical materials, welding, metal refining, textiles, lubricating oil additives, and insulation. It is also known as the mineral potassium pentaborate ($KB_5O_8{\cdot}4H_2O$), which has an orthorhombic lattice system called santite, and whose crystals appear as transparent and colorless aggregates (Asensio et al., 2016; Dumanlı et al., 2021; Merlino and Sartori, 1970; T.R. Prime Ministry SPO, 2006; Thamizharasan et al., 2000; Yang et al., 2005).

In the ultrasonic chemical reactions, a multi-bubble environment is created, which leads to a strong and rapid connection of the reactants in which acoustic cavitations are formed by kinetic energy supplied. Hence, this acoustic cavitation provides high pressure, high temperature, and high energy levels to the raw materials in a very short period thus accelerating the reactions and leading to high reaction efficiencies (Lupacchini et al., 2017; Mettin et al., 2015; Timothy, 2017). Several boron minerals were obtained in the literature by using ultrasonic synthesis such as magnesium borates (Kipcak et al., 2014; Kipcak and Derun, 2016), $NaB(OH)_4{\cdot}2H_2O$ (Yilmaz et al., 2012), and zinc borates (Dumanli et al., 2020; Ersan et al., 2016, 2020; Vardar et al., 2017). Other than ultrasonic synthesis, there are several syntheses of potassium borate studies such as KB_5 (Karagöz and Kuşlu, 2021), $KB_5O_7(OH)_2{\cdot}H_2O$ (Zhang et al., 2005), $KB_3O_5{\cdot}3H_2O$ (Salentine, 1987), $KB_5O_7(OH)_2$ (Wu, 2011), $KB_3O_4(OH)_2$ (Wang et al., 2006); $K_2B_5O_8(OH){\cdot}2H_2O$ (Liu et al., 2007), and $KB_5O_8{\cdot}4H_2O$ (Asensio et al., 2016; İla et al., 2020; Dumanlı et al., 2021).

As it is seen from the given literature, the ultrasonic synthesis of the potassium borates is not studied. In this study, ultrafast and effective ultrasonic synthesis of potassium borate mineral "santite" was aimed. For this aim, eight different raw material combinations and four different reaction temperatures along with four reaction times were conducted. X-ray diffraction (XRD) and Raman spectroscopy techniques were used for the characterization of synthesized products. Morphological analyses were conducted using scanning electron microscopy (SEM) and overall reaction yields were calculated.

* **Corresponding author: Emek Moroydor Derun,** Chemical Engineering Department, Yildiz Technical University, Faculty of Chemical and Metallurgical Engineering, Istanbul, Turkey, e-mail: moroydor@yildiz.edu.tr
Sibel İla, Azmi Seyhun Kipcak: Chemical Engineering Department, Yildiz Technical University, Faculty of Chemical and Metallurgical Engineering, Istanbul, Turkey

2 Results

2.1 XRD results of synthesized products

The product of santite is synthesized with the formulae and powder diffraction file no. of "$KB_5O_8{\cdot}4(H_2O)$" and "01-072-1688", respectively. Obtained product was the same as given given in the studies of Asensio et al. (2016), Dumanlı et al. (2021), and İla et al. (2020). In Table 1, XRD scores of the synthesized santite mineral are given, where XRD scores of the analyzed mineral are equal to 100 when all of the peak intensities (%) and peak locations matched perfectly with the pdf card number of the reference mineral (Ibroska et al., 2015; Sari et al., 2017).

In Set-1, where the raw materials of K_2CO_3 and H_3BO_3 were used with a boron/potassium mole ratio of 5, the highest XRD score was obtained at 60°C in the reaction time of 5 min, with an XRD score of 75. In Set-2, the raw materials of K_2CO_3 and B_2O_3 were used with a boron/potassium mole ratio of 6, and the highest XRD score was obtained at 70°C in the reaction time of 10 min, with an XRD score of 60. The raw materials of KNO_3, NaOH, and H_3BO_3 were used with a boron/potassium mole ratio of 6 in Set-3, and 68 XRD score was obtained at 60°C in the reaction time of 10 min. The raw materials of KNO_3, NaOH, and B_2O_3 were used with a boron/potassium mole ratio of 6 in Set-4, and a 51 XRD score was obtained at 90°C in the reaction time of 2.5 min. In Set-5, where the raw materials of KNO_3, $Na_2B_4O_9{\cdot}5H_2O$, and H_3BO_3 were used with a boron/potassium mole ratio of 6, the highest XRD score was obtained at 60°C in the reaction time of 2.5 min, with the XRD score of 63. In Set-6, where the raw materials of KNO_3, $Na_2B_4O_9{\cdot}5H_2O$, and B_2O_3 were used with a boron/potassium mole ratio of 6, the highest XRD score was obtained at 60°C in the reaction time of 15 min, with the XRD score of 54. The raw materials of KNO_3, $Na_2B_4O_9{\cdot}10H_2O$, and H_3BO_3 were used with a boron/potassium mole ratio of 5 in Set-7, and 60 XRD score was obtained at 80°C in the reaction time of 2.5 min. In the last Set-8, the raw materials of KNO_3, $Na_2B_4O_9{\cdot}10H_2O$, and B_2O_3 were used with a boron/potassium mole ratio of 7, and 61 XRD score was obtained at 60°C in the reaction time of 2.5 min.

Table 1: XRD scores of the synthesized santite minerals

SET		Reaction time (min)	Reaction temperature (°C)			
			60	70	80	90
1	KC–H	15	70	33	44	37
		10	64	49	41	49
		5	**75**	62	43	37
		2.5	70	39	28	35
2	KC–B	15	54	50	45	40
		10	55	**60**	35	44
		5	55	42	44	25
		2.5	56	42	30	32
3	KN–N–H	15	61	46	40	27
		10	**68**	60	53	47
		5	49	40	39	48
		2.5	44	37	39	53
4	KN–N–B	15	42	38	36	34
		10	38	32	40	46
		5	44	36	44	44
		2.5	45	34	40	**51**
5	KN–T–H	15	49	37	45	48
		10	60	27	40	41
		5	62	33	53	31
		2.5	**63**	31	55	45
6	KN–T–B	15	**54**	40	42	42
		10	51	46	51	38
		5	32	27	50	36
		2.5	47	33	51	44
7	KN–BX–H	15	43	46	43	47
		10	38	43	46	20
		5	34	45	49	49
		2.5	36	32	**60**	49
8	KN–BX–B	15	59	36	43	33
		10	59	39	43	51
		5	48	49	41	41
		2.5	**61**	39	41	48

2.2 Raman spectroscopy results

All obtained Raman spectra are very similar, hence in Figure 1, only Raman spectra of KC–H set at 60°C reaction temperature are given. No peak was observed between 3,280 and 1,600 cm^{-1} Raman shift in the Raman spectra of potassium borate of "santite," so the Raman shift range was given from 1,600 to 250 cm^{-1}.

According to the obtained Raman spectra, the band seen between 916 and 918 cm^{-1} was the symmetrical stretching of 3 coordinated boron with oxygen [$\nu_s(B_{(3)}–O)$]. Symmetric stretching of 4 coordinated boron with oxygen [$\nu_s(B_{(4)}–O)$] was obtained between 786 and 764 cm^{-1}. The band seen at 555 cm^{-1} was the boron compound's characteristic peak of [$\nu_p[B_4O_5(OH)_4]^{-2}$] and was due to the combination of two BO_3 planar triangles and two BO_4 tetrahedrons. Another boron compound's characteristic peak of [$\nu_p[B_5O_6(OH)_4]^{-}$] was obtained between the band values of 508–506 cm^{-1} and was due to the combination of two BO_3 planar triangles and a BO_4 tetrahedron. The band seen between 457 and 455 cm^{-1} was the bending of 4 coordinated boron with oxygen [$\delta(B_{(4)}–O)$].

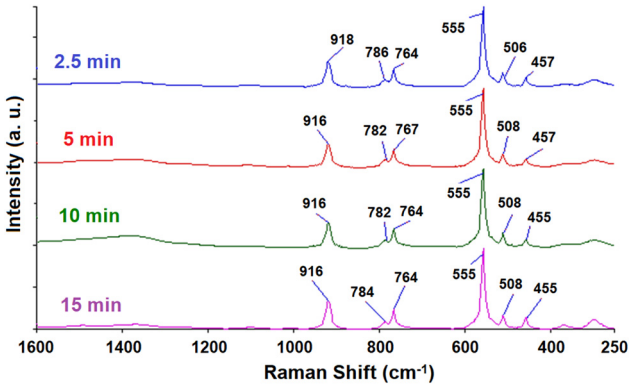

Figure 1: Raman spectra of the santite synthesized at KC–H set at 60°C reaction temperature.

2.3 SEM morphology results

SEM morphologies of the highest XRD scored products are given in Figure 2.

According to the SEM image of the KC–H set, where santite was obtained at 60°C reaction temperature and 5 min reaction time, the particle size of the synthesis product ranges from 790 nm to 1.02 µm, in which the particles had sharp angular lines and some agglomerations occurred. In the SEM morphology of the KC–B set, where santite was obtained at 70°C reaction temperature and 10 min reaction time, the particle sizes were between 305 nm and 1.50 µm, and more sharp rectangular particles occurred rather than the angular lines obtained from KC-T set with more agglomerations. In the set of KN–N–H, where santite was obtained at 60°C reaction temperature and 10 min reaction time, the particle sizes were between 560 nm and 1.87 µm, in which the particles have a more rounded structure compared to the KC–H and KC–B sets, and fewer agglomerations were observed in the structure. In the set of KN–N–B, where santite was obtained at 90°C reaction temperature and 2.5 min reaction time, the particle sizes were between 551 nm and 1.42 µm, in which angular and round particles were obtained together with some agglomeration. In the set of KN–T–H, where santite was obtained at 60°C reaction temperature and 2.5 min reaction time, obtained particles were seen as agglomerated sharp triangular and rectangular shapes with the particle sizes between 515 nm and 2.00 µm. In the set of KN–T–B, where santite was obtained at 60°C reaction temperature and 15 min reaction time, the obtained particles agglomerated partly in sharp lines and partly round shapes, with the particle sizes between 384 nm and 1.25 µm. In the set of KN–BX–H, where santite was obtained at 80°C reaction temperature and 2.5 min reaction time, triangular sharp formations with agglomeration were observed with particle sizes between 589 nm and 1.47 µm. In the last set of KN–BX–B, where santite was

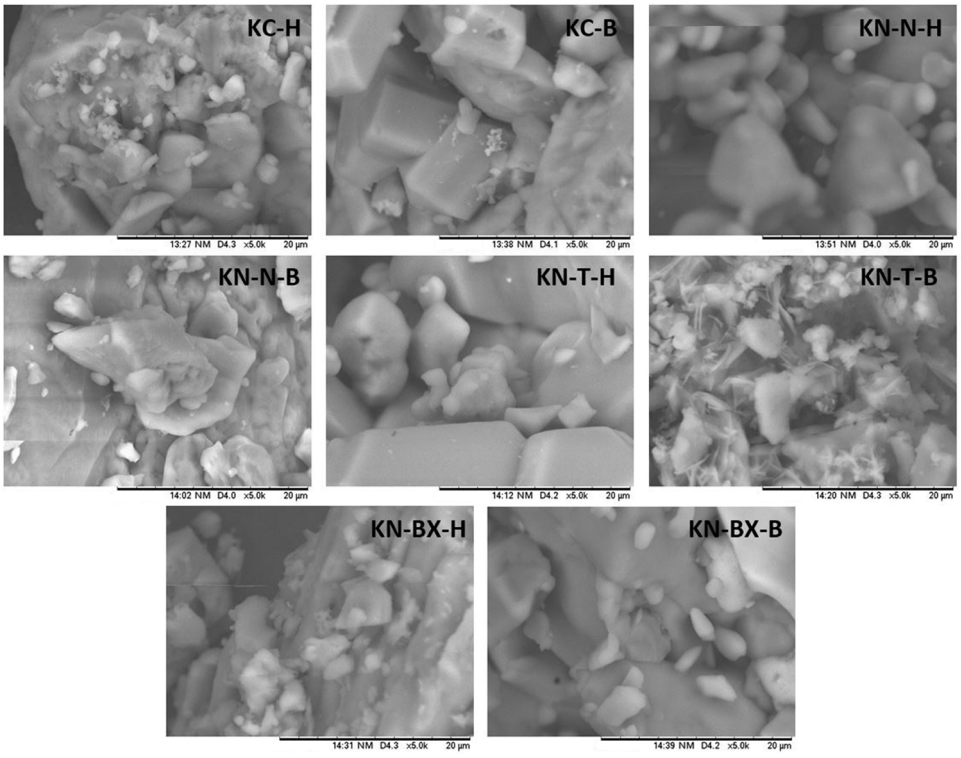

Figure 2: SEM morphologies of the highest XRD scored synthesized santite.

obtained at 60°C reaction temperature and 2.5 min reaction time, agglomerated round formations were seen with particle sizes between 554 nm and 2.03 µm.

2.4 Overall santite yields

Overall santite reaction yields (%) with respect to reaction temperature and time are given in Figure 3. According to the obtained overall santite yield results, in general, reaction yields increased with increasing reaction temperature and reaction time. Higher reaction yields were seen at the raw material combinations of KN–T–H, KN–T–B, KN–BX–B. The reaction yields were found between 87.20–92.12%, 76.11–84.41%, 84.45–98.94%, 91.92–97.87%, 90.15–99.07%, 94.46–99.26%, 90.12–96.50%, and 90.13–98.94% for the sets of KC–H, KC–B, KN–N–H, KN–N–B, KN–T–H, KN–T–B, KN–BX–H, and KN–BX–B, respectively.

3 Discussion

It was seen that K_2CO_3 leads to higher XRD scores than KNO_3 and H_3BO_3 leads to higher XRD scores than B_2O_3. In

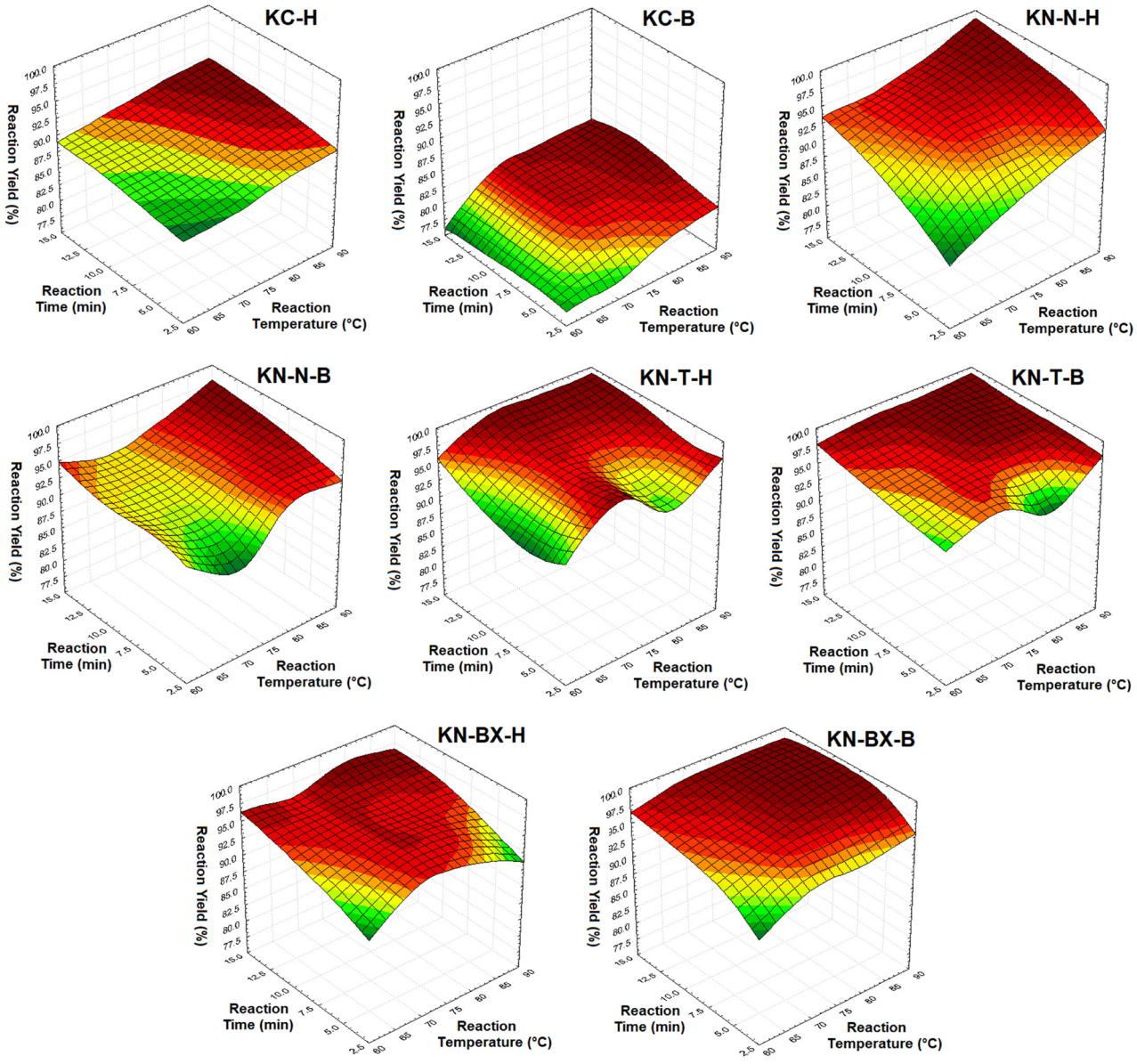

Figure 3: Overall reaction yields of santite synthesized in different sets.

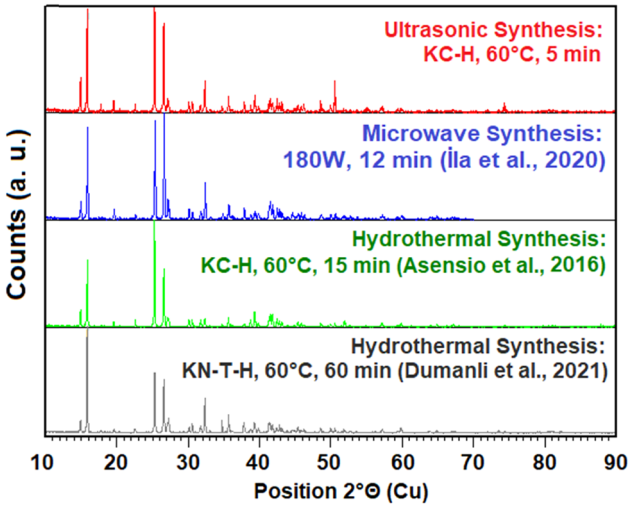

Figure 4: XRD pattern of the highest XRD scored santite, and comparison with the literature.

Table 2, XRD Scores of the literature studies taken from Asensio et al. (2016) and Dumanlı et al. (2021) are given for the comparison with this study (Figure 4). Furthermore, for comparison with the hydrothermal studies of Asensio et al. (2016) and Dumanlı et al. (2021), Table 2 is prepared. As seen in Table 2, obtained XRD scores in this study were a little lower than the hydrothermal studies but ultrasonic irradiation led to the rapid formation of santite, which provides more energy-saving and the process turns into green synthesis.

The obtained band was in mutual agreement with the studies of Asensio et al. (2016), Dumanlı et al. (2021), and İla et al. (2020).

SEM morphologies showed that by using the ultrasonic method, different raw material combinations yield different particle formations with reduced particle sizes ranging from 305 nm to 2.03 µm compared with the literature. In the hydrothermal synthesis studies, Asensio et al. (2016) found that the santite particle sizes are between 667.67 nm and 5.98 µm, Dumanlı et al. (2021) found that the santite particle sizes are between 234.94 nm and 3.41 µm. In the microwave synthesis studies, İla et al. (2020) found that the santite particle sizes are between 717 nm and 2.63 µm.

In the literature, santite yields were given between 65.5 and 69.2% for microwave synthesis (İla et al., 2020) and 80–99% for hydrothermal studies (Asensio et al., 2016; Dumanlı et al., 2021). The ultrasonic method had better reaction yields than microwave synthesis and a little lower than hydrothermal synthesis. On the other hand, ultrasonic synthesis has a slower reaction time (2.5–15 min) than hydrothermal studies (30–240 min).

4 Conclusions

In this study from different potassium (K_2CO_3 and KNO_3) and boron sources (H_3BO_3, B_2O_3, $Na_2B_4O_9{\cdot}5H_2O$, and KNO_3-$Na_2B_4O_9{\cdot}10H_2O$), a potassium borate mineral of santite ($KB_5O_8{\cdot}4H_2O$) was synthesized by using ultrasonic method between the reaction temperatures of 60–90°C and 2.5–15 min reaction times. Synthesized santite minerals are characterized by XRD and Raman spectroscopy techniques and the compound's XRD pattern and Raman spectroscopy were in mutual agreement with the literature. From the SEM morphological analysis, the particle size of the santite was between 305 nm and 2.03 µm. Furthermore, overall santite yields, even with such lower reaction times compared with the literature, are found between 76.11% and 99.26%. As a result, ultrafast and effective synthesis of santite is possible by using the ultrasonic synthesis method.

5 Experimental

5.1 Preparation of raw materials

K_2CO_3 (99%) and KNO_3 (99%), which were used as potassium sources in the ultrasonic synthesis studies, were obtained from Sigma-Aldrich (Sigma-Aldrich Chemie

Table 2: Santite minerals' highest XRD scores, with respect to reaction temperature and time, given in the literature

SET		Reaction temperature (°C)	Reaction time (min)	XRD score	Reference
1	KC–H	60	15	74	Asensio et al., 2016
2	KC–B	70	30	63	Asensio et al., 2016
3	KN–N–H	60	60	75	Dumanlı et al., 2021
4	KN–N–B	60	60	72	Dumanlı et al., 2021
5	KN–T–H	60	60	77	Dumanlı et al., 2021
6	KN–T–B	70	30	69	Dumanlı et al., 2021
7	KN–BX–H	70	120	72	Dumanlı et al., 2021
8	KN–BX–B	80	30	73	Dumanlı et al., 2021

GmbH, Taufkirchen, Germany) and Merck chemicals (Merck KGaA, Darmstadt, Germany), respectively. H_3BO_3 (99.9%) and B_2O_3 (98%) were used as boron sources, borax ($Na_2B_4O_7{\cdot}10H_2O$, 99.9%) and tinkalkonite ($Na_2B_4O_7{\cdot}5H_2O$, 99.9%) were used as the sources of boron and sodium, which were retrieved from Bandırma Boron Works (Eti Maden, Balıkesir, Turkey), under the titles of Etiboric Acid, Etiboroxide, Borax Decahydrate, and Borax Pentahydrate, respectively. Boron sources were used with a grain size of <75 μm (over 200 mesh) by going through the crushing, grinding, and screening stages, respectively. NaOH (98%), the source of sodium, was obtained from Merck chemicals (Merck KgaA, Darmstadt, Germany).

5.2 Ultrasonic synthesis

The raw material combinations and ratios used were the same as the hydrothermal studies of Asensio et al. (2016) and Dumanlı et al. (2021) and are given in Table 3.

For each set, the same reactor as in the studies of Asensio et al. (2016) and Dumanlı et al. (2021) was used, and the reaction parameters were selected as 60°C, 70°C, 80°C, and 90°C reaction temperatures and 15, 10, 5, 2.5 min reaction times. The pure water used in the experiments was obtained with the "GFL 2004 (Gesselschaft für Labortechnik, Burgwedel, Germany)" brand water purification system and its pH value was measured as 5.5. For the mixing process, Bandelin Sonopuls HD 2070 ultrasonic homogenizer (Bandelin electronic GmbH & Co. KG, Berlin, Germany) was used at 80% cycle and 90% power (Dumanli et al., 2020; Ersan et al., 2016, 2020; Kipcak and Derun, 2016; Vardar et al., 2017). After the determined reaction time, the reactor was opened and products and unreacted raw materials were placed in a glass crystallizer then put in a 40°C oven (Ecocell LSIS-B2V/EC55; MMM Medcenter Einrichtungen, Planegg, Germany) for potassium borate crystals to occur and evaporation of excess water. After 12 h, the obtained products were washed with 96% pure ethanol (Merck KgaA, Darmstadt, Germany) to remove the unreacted raw materials and formed $NaNO_3$ by-products. Finally, excess ethanol was evaporated in the same oven. Detailed chemical reactions were given in the studies of Asensio et al. (2016) and Dumanlı et al. (2021).

Table 3: Raw material combinations used in the ultrasonic synthesis of potassium borates (Asensio et al., 2016; Dumanlı et al., 2021)

Set #	Code	Raw materials	B:K ratio
1	KC–H	K_2CO_3–H_3BO_3	5
2	KC–B	K_2CO_3–B_2O_3	6
3	KN–N–H	KNO_3–NaOH–H_3BO_3	6
4	KN–N–B	KNO_3–NaOH–B_2O_3	6
5	KN–T–H	KNO_3–$Na_2B_4O_9{\cdot}5H_2O$–H_3BO_3	6
6	KN–T–B	KNO_3–$Na_2B_4O_9{\cdot}5H_2O$–B_2O_3	6
7	KN–BX–H	KNO_3–$Na_2B_4O_9{\cdot}10H_2O$–H_3BO_3	5
8	KN–BX–B	KNO_3–$Na_2B_4O_9{\cdot}10H_2O$–B_2O_3	7

5.3 Characterization of the synthesized products

Identification of the samples was made with the X-rays created in the Cu-Kα (λ = 0.153 nm) tube at 45 kV and 40 mA parameters ($7 < 2\Theta < 90$) in the XRD equipment (PANalytical B.V., Almelo, The Netherlands).

After XRD analysis, products were analyzed with the Raman spectroscopy technique for the specific bands of the samples under the visible region with the parameters of 4 s experiment period and four repetitions in the range of 3,280–250 cm^{-1} on the Perkin Elmer Raman Station 400 F (PerkinElmer, MA, USA).

For surface morphology analysis of the synthesis products, the Hitachi TM3030Plus SEM device (Hitachi Ltd. Corporation, Tokyo, Japan) was used. Analyses were made at 15 kV and the imaging and magnifications set were 5,000.

5.4 Reaction yields

Reaction yield based on moles and the overall yield, Y_D, is defined as the ratio of moles of product formed at the end of the reaction, N_D, to the number of moles of limiting reactant, A, that have been consumed. N_{A0} and N_A are the initial and final moles of consumed reactants, respectively. For a batch system (Dumanlı et al., 2021):

$$Y_D = \frac{N_D}{N_{A0} - N_A} \quad (1)$$

Three parallel syntheses were conducted for the calculation as average reaction yields, where K_2CO_3 and KNO_3 were selected as the limiting reactants.

Funding information: Authors state no funding involved.

Author contributions: Sibel İla: experiments; Azmi Seyhun Kipcak: experiments, instrumental analysis, writing – original

draft; Emek Moroydor Derun: methodology, project administration, writing – original draft, writing – review and editing.

Conflict of interest: Authors state no conflict of interest.

References

Asensio M.O., Yildirim M., Senberber F.T., Kipcak A.S., Derun E.M., Thermal dehydration kinetics and characterization of synthesized potassium borates. Res. Chem. Intermediat., 2016, 42(5), 4859–4878.

Dumanli F.T.S., Kipcak A.S., Vardar D.S., Tugrul N., Ultrasonic-assisted synthesis of zinc borates: effect of boron sources. J. Chem. Soc. Pak., 2020, 42(6), 839–845.

Dumanlı F.T.S., Ozen M.Y., Asensio M.O., Yuksel S.A., Kipcak A.S., Derun E.M., Characteristic, electrical and optical properties of potassium borate ($KB5O8{\cdot}4H_2O$) hydrothermally synthesised from different boron sources. Res. Chem. Intermediat., 2021, 47, 5353–5368.

Ersan A.C., Kipcak A.S., Ozen M.Y., Tugrul N., An accelerated and effective synthesis of zinc borate from zinc sulfate using sonochemistry. Main. Group. Met. Chem., 2020, 43, 7–14.

Ersan A.C., Yildirim M., Kipcak A.S., Tugrul N., A novel synthesis of zinc borates from a zinc oxide precursor via ultrasonic irradiation. Acta Chim. Slov., 2016, 63, 881–890.

Ibroska T., Kipcak A.S., Yuksel S.A., Derun E.M., Piskin S., Synthesis, characterization, and electrical and optical properties of magnesium-type boracite. Turk. J. Chem., 2015, 39(5), 1025–1037.

İla S., Kipcak A.S., Derun E.M., A new rapid synthesis of potassium borates by microwave irradiation. Main. Group. Chem., 2020, 19(4), 265–272.

Karagöz Ö., Kuşlu S., Synthesis of pure potassium pentaborate (KB_5) from potassium dihydrogen phosphate (KH_2PO_4) and colemanite. Chem. Pap., 2021, 75, 5963–5969.

Kipcak A.S., Derun E.M., A new approach on the evaluation of magnesium wastes in the magnesium borate synthesis using the novel method of ultrasonic irradiation. Res. Chem. Intermediat., 2016, 42(8), 6663–6679.

Kipcak A.S., Derun E.M., Piskin S., Synthesis and characterization of magnesium borate minerals of admontite and mcallisterite obtained via ultrasonic mixing of magnesium oxide and various sources of boron: a novel method. Turk. J. Chem., 2014, 38(5), 792–805.

Liu Z.H., Li P., Li L.Q., Jia Q.X., Synthesis, characterization and thermochemistry of $K_2B_5O_8(OH){\cdot}2H_2O$. Thermochim. Acta., 2007, 454, 23–25.

Lupacchini M., Mascitti A., Giachi G., Tonucci L., d'Alessandro N., Martinez J., et al., Sonochemistry in non-conventional, green solvents or solvent-free reactions. Tetrahedron. 73, 2017, 609–653.

Merlino S., Sartori F., Santite, a new mineral phase from Larderello, Tuscany. Contr Miner. Pet., 1970 27, 159–165.

Mettin R., Cairós C., Troia A., Sonochemistry and bubble dynamics. Ultrason. Sonochem., 2015, 25, 24–30.

Salentine C.G., Synthesis, characterization, and crystal structure of a $KB_3O_5{\cdot}3H_2O$, Inorg. Chem., 1987, 26(1), 128–132.

Sari S., Senberber F.T., Yıldırım M., Kıpçak A.S., Yuksel S.A., Derun E., Lanthanum borate synthesis via the solid-state method from a La_2O_3 precursor: electrical and optical properties. Mater. Chem. Phys., 2017, 200:196–203.

T.R. Prime Ministry SPO, Chemical industry private expertise commission, boron operations group report: ninth development plan (2007–2013), Turkey: T.R. Prime Ministry SPO,2006.

Thamizharasan K., Jesu Raja S.X., Xavier F.P., Sagayaraj P., Growth, thermal and microhardness studies of single crystals of potassium penta borate (KB5). J. Cryst. Growth., 2000, 218(2–4), 323–326.

Timothy J.M., Sonochemistry and sonoprocessing: the link, the trends and (probably) the future. Ultrason. Sonochem., 2017, 10, 175–179.

Vardar D.S., Senberber F.T., Kipcak A.S., Tugrul N., A green sonochemical synthesis of zinc borates from $Zn_5(CO_3)_2{\cdot}(OH)_6$. Main. Group. Chem., 2017, 16, 163–173.

Wang G.M., Sun Y.Q., Zheng S.T., Yang G.Y., Synthesis and crystal structure of a novel potassium borate with an unprecedented $[B_{12}O_{16}(OH)_8]^{4-}$ anion. Z. Anorg. Allg. Chem., 2006, 632(8–9), 1586–1590.

Wu Q. Potassium pentaborate, Acta Cryst., 2011, E67, i67.

Yang G., Li Z., Zhang Y., Dehydration of tetrahydrate potassium pentaborate in fluidized bed. Chem. Eng. Process., 2005, 44(11), 1216–1220.

Yilmaz M., Figen A., Piskin S., Production of sodium metaborate tetrahydrate ($NaB(OH)_4{\cdot}2H_2O$) using ultrasonic irradiation. Powder Technol., 2012, 215–216, 166–173.

Zhang H.X., Zhang J., Zheng S.T., Yang G.Y., Two new potassium borates, $K_4B_{10}O_{15}(OH)_4$ with stepped chain and $KB_5O_7(OH)_2{\cdot}H_2O$ with double helical chain. Cryst. Growth Des., 2005, 5(1), 157–161.